:UMENTATION PAGE

Form Approved
OMB No. 0704-0188

ition is estimated to average 1 hour per response, including the time for reviewing instructions, searching existing data sources, gathering and reviewing the collection of information. Send comments regarding this burden estimate or any other aspect of this reducing this burden, to Washington Headquarters Services, Directorate for information Operations and Reports, 1215 Jefferson 2, and to the Office of Management and Budget, Paperwork Reduction Project (0704-0188), Washington, DC 20503.

2. REPORT DATE: February 18, 1994
3. REPORT TYPE AND DATES COVERED: Reprint

(2)

4. TITLE AND SUBTITLE

Guided-ion Beam Measurements of the $X^+ + H_2O(D_2O)$ X=Ar,N_2) Collision Systems

5. FUNDING NUMBERS

PE 61102F
PR 2303
TA G2
WU 01

6. AUTHOR(S)

Rainer A. Dressler, Richard H. Salter, Edmond Murad

7. PERFORMING ORGANIZATION NAME(S) AND ADDRESS(ES)

Phillips Lab/WSSI
29 Randolph Road
Hanscom AFB, MA 01731-3010

8. PERFORMING ORGANIZATION REPORT NUMBER

PL-TR-94-2030

9. SPONSORING/MONITORING AGENCY NAME(S) AND ADDRESS(ES)

10. SPONSORING/MONITORING AGENCY REPORT NUMBER

11. SUPPLEMENTARY NOTES

Reprinted from J. Chem. Phys. 99 (2), 15 July 1993

12a. DISTRIBUTION/AVAILABILITY STATEMENT

Approved for public release; Distribution unlimited

13. ABSTRACT (Maximum 200 words)

Guided-ion beam cross section and product kinetic energy measurements of charge-transfer and atom-abstraction reactions of the $Ar^+ + H_2O(D_2O)$ and $N_2^+ + H_2O(D_2O)$ collision systems are presented for collision energies ranging between 0.2 and 20 eV c.m. Both charge-transfer systems exhibit large hyperthermal cross sections exceeding 10 $Å^2$ and are characterized by a long-range interaction, evidenced by the small amount of angular scattering observed in product-ion time-of-flight (TOF) measurements. Weak forward-scattered signals due to orbiting collisions are detected and are interpreted to stem from a dipole orientation that maximizes the long-range attractive forces. The charge-transfer product ion velocity distributions are well described by an osculating complex model. The charge-transfer systems exhibit weak isotope effects that are related to competition with the atom-abstraction channels. The atom-abstraction cross sections represent ~10% of the total cross section and the observed distinct isotope effects and TOF distributions are consistent with a pairwise-energy model.

14. SUBJECT TERMS

Guided-ion beam; Charge-transfer; Ion-molecule interactions; Cross section; Water; Energy partitioning; Time of flight

15. NUMBER OF PAGES: 13

16. PRICE CODE

17. SECURITY CLASSIFICATION OF REPORT	18. SECURITY CLASSIFICATION OF THIS PAGE	19. SECURITY CLASSIFICATION OF ABSTRACT	20. LIMITATION OF ABSTRACT
UNCLASSIFIED	UNCLASSIFIED	UNCLASSIFIED	SAR

Guided-ion beam measurements of the $X^+ + H_2O(D_2O)$ ($X = Ar, N_2$) collision systems

Rainer A. Dressler, Richard H. Salter, and Edmond Murad
Phillips Laboratory, Spacecraft Interactions Branch, PL/WSSI, Hanscom AFB, Massachusetts 01731

(Received 11 March 1993; accepted 5 April 1993)

Guided-ion beam cross section and product kinetic energy measurements of charge-transfer and atom-abstraction reactions of the $Ar^+ + H_2O(D_2O)$ and $N_2^+ + H_2O(D_2O)$ collision systems are presented for collision energies ranging between 0.2 and 20 eV c.m. Both charge-transfer systems exhibit large hyperthermal cross sections exceeding 10 Å^2 and are characterized by a long-range interaction, evidenced by the small amount of angular scattering observed in product-ion time-of-flight (TOF) measurements. Weak forward-scattered signals due to orbiting collisions are detected and are interpreted to stem from a dipole orientation that maximizes the long-range attractive forces. The charge-transfer product ion velocity distributions are well described by an osculating complex model. The charge-transfer systems exhibit weak isotope effects that are related to competition with the atom-abstraction channels. The atom-abstraction cross sections represent ~10% of the total cross section and the observed distinct isotope effects and TOF distributions are consistent with a pairwise-energy model.

I. INTRODUCTION

Water is a major constituent of the artificial atmosphere surrounding spacecraft in low-Earth orbit.[1,2] Spacecraft and this atmosphere travel at a velocity of ~7.8 km s^{-1}. Hyperthermal charge-transfer collisions between atmospheric ions and H_2O are, therefore, a major source of ionization in the spacecraft environment.[3,4] Ion–H_2O reactions are also of interest from a chemical-kinetic point of view. They can be regarded as prototypes of ion–polyatomic molecule reactions because the two simplest ion–molecule reaction processes, charge transfer and hydrogen-atom abstraction, can be studied simultaneously.

In the $Ar^+ + H_2O$ and $N_2^+ + H_2O$ collision systems, both charge transfer and hydrogen-atom abstraction are exothermic,

$$Ar^+ + H_2O(D_2O) \rightarrow Ar + H_2O^+(D_2O^+) + 3.14 \text{ eV} \quad (1)$$

$$\rightarrow ArH^+(ArD^+) + OH(OD) + 0.9 \text{ eV}, \quad (2)$$

$$N_2^+ + H_2O(D_2O) \rightarrow N_2 + H_2O^+(D_2O^+) + 2.96 \text{ eV} \quad (3)$$

$$\rightarrow N_2H^+(N_2D^+) + OH(OD) + 1.9 \text{ eV}, \quad (4)$$

and they are, therefore, expected to compete at low collision energies. The dynamics of these systems are particularly interesting due to two low-lying electronic states of the charge-transfer product, H_2O^+. These states have markedly different equilibrium geometries, the $\tilde{X}\,^2B_1$ ground state is bent, and the first excited $\tilde{A}\,^2A_1$ state is linear. Since the $\tilde{A}\,^2A_1$ state lies only 1 eV above the ground state, both Ar^+ and N_2^+ have sufficiently high recombination energies to access the $\tilde{A}$-state charge-transfer surface without requiring translational energy transfer.

Recently, we have reported the observation of H_2O^+ $\tilde{A}\,^2A_1$–$\tilde{X}\,^2B_1$ luminescence from the $Ar^+ + H_2O$ and $N_2^+ + H_2O$ collision systems.[5,6] The analysis of the spectra provided exceptional insight into the validity of energy-resonance and Franck–Condon criteria[7,8] for the prediction of state-to-state cross sections. The luminescence experiment also revealed OH $A\,^2\Sigma^+$–$X\,^2\Pi$ chemiluminescence from the hydrogen-atom abstraction reactions observed in the same collision systems.[9] The rotational energy distribution of the OH A state deduced from the chemiluminescence spectra demonstrated the importance of the charge-transfer surface in ion–molecule chemical reactivity.

Previous experimental studies of the charge-transfer systems (1) and (3) have exhibited hyperthermal cross sections exceeding 10 Å^2.[10,11] The large charge-transfer cross sections indicate that the nonadiabatic transitions occur at long range. Consequently, primarily large impact parameter collisions lead to charge transfer and the incident projectile barely experiences a deflection in the collision. The product H_2O^+ ions are, therefore, produced with predominantly near-thermal translational energies in ion-beam experiments involving thermal water vapor. This has been confirmed by crossed-beam experiments of the $Ar^+ + H_2O$ system by Glosik *et al.*[12] and time-of-flight (TOF) measurements conducted in a tandem-mass spectrometer system for the $N_2^+ + H_2O$ system.[11]

Reliable cross sections of product channels exhibiting large-angle scattering can only be obtained from an experiment that efficiently collects the product ions without affecting the field-free conditions of the collision region. The past $Ar^+ + H_2O$ and $N_2^+ + H_2O$ charge-transfer cross section measurements depended on the correct assessment of the collection efficiency and the assumption that the product ions were scattered isotropically in the laboratory (LAB) frame.[10,11]

While arguably a valid assumption for the charge-transfer systems, this assumption is far riskier for hyper-

 0021-9606/93/99(2)/1159/13/$6.00

thermal atom-abstraction channels because these reactions are expected to proceed at shorter range, thus causing some large-angle scattering in the center-of-mass (CM) frame. The earlier molecular dynamic studies of these reactions have found the atom-abstraction channels to proceed via a spectator-stripping mechanism producing strongly forward-scattered product ions.[11,12] The substantial OH A–X chemiluminescence intensities, the production of which is endothermic by 3.1 eV in reaction (2) and 2.1 eV in reaction (4), indicates, however, that energy transfer accompanied by large-angle scattering is more efficient in these reactions than suggested by the spectator-stripping model.[9]

In order to overcome the uncertainty of product-ion collection, we have recently constructed a guided-ion beam (GIB) apparatus for the study of ion-neutral collisions from near-thermal to hyperthermal collision energies. The now widely used GIB technique is based on the ion-trapping properties of inhomogeneous radio-frequency (rf) fields.[13,14] In carrying out the ion–molecule reaction in a cylindrical ion trap consisting of a rf-only octopole system, product ions are collected irrespective of the scattering angle, and reactions can be studied over collision energies ranging from thermal to hyperthermal energies with equal sensitivity. Since properly operated octopoles exhibit excellent energy conserving properties, TOF measurements can be carried out over long low-energy flight paths, presenting an ideal tool for the study of product kinetic energy distributions, and therefore energy partitioning in ion–molecule reactions. The superiority of the GIB technique over the instrumentation previously used to study the ion–water systems (1)–(4) warrants a reinvestigation of these reactions.

In this paper, we present GIB cross-section and product-ion TOF measurements for reactions (1)–(4). The new GIB experiment is described in Sec. II. The energy dependence of the measured cross sections and product-ion velocity distributions determined from TOF measurements are presented in Sec. III. In a previous communication, we have demonstrated the merits of the osculating complex model[15,16] in interpreting the $O^+ + H_2O$ charge-transfer product-ion velocity distributions.[17] It is shown that this model also applies adequately to the charge-transfer (1) and (3) systems. The results are discussed in Sec. IV, and compared to recent optical measurements.[6,9]

II. EXPERIMENT

The apparatus is a previously described tandem mass spectrometer[11] in which the former collision cell and associated ion optics have been replaced by an octopole ion-guide system. An ion beam is produced in an electron-impact ion source. The electron energy is kept as low as possible to avoid metastable ion production. In the case of N_2^+, ~20% of the ions are expected to be vibrationally excited.[18] A statistical distribution of $Ar^+(^2P_j)$ spin–orbit states is assumed. The ion beam is accelerated into a Wien velocity filter for mass selection. Following deceleration, the beam is injected into a first 7.36 cm long octopole ion-beam guide of 0.6 cm inner diameter and 0.2 cm rod diameter. A schematic of the ion-guide system is shown in Fig. 1. The design is similar to octopole systems described by Gerlich and co-workers.[14,19–21] The first octopole passes through a 3.5 cm long collision cell containing the neutral target gas. The target gas pressure is measured with a capacitance manometer and is adjusted to be between 0.15 and 0.2 mTorr. At the collision cell exit end, primary and product ions enter a second octopole ion-beam guide of equal radial dimension, but of 16.73 cm length. A four-element lens accelerates primary and secondary ions from the exit end of the second octopole and focuses them into a quadrupole mass filter. Following mass analysis, the ions are detected using a channel electron multiplier or channel-plate detector. The pulses from the detector are processed and counted with a PC-based multichannel scaler.

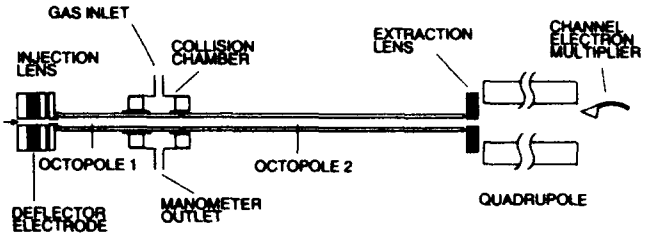

FIG. 1. Schematic representation of the interaction region of the guided-ion beam experiment. Generation of the mass-selected energy beam is identical to that described in a previous publication (Ref. 11).

The 10 MHz sine-wave output of a function generator is amplified with a linear rf amplifier and coupled to the octopole rods using an antiresonant LC tank circuit and associated electronics. An amplifier output of 10 W typically yields a 120 V rf amplitude. The guiding field generated by the rf voltage traps the ions in the radial direction without significantly affecting the ion translational energy.[13,14] The two octopoles have the same rf phase but the dc-bias potential of the second octopole is reduced with respect to that of the first octopole by ~200–400 mV. This slightly accelerates the product ions in order to avoid trapping of very slow ions by potential barriers due to inhomogeneities of the octopole rod surface potentials. The collision chamber potential is equal to the bias potential of the first octopole. Ions that are scattered backwards in the LAB frame can be reflected into the forward direction by a positive potential at the injection electrode, or by applying a positive potential to a cylindrical electrode surrounding the octopole at the entrance of the collision cell. The applied voltage generates a potential barrier within the octopole that is small enough not to significantly affect the collision energy distribution, but large enough to reflect slow backscattered ions into the forward direction.

The octopole system can be biased up to 200 V above the quadrupole dc-bias potential. In this work it has been found that product and primary ions are collected efficiently at octopole dc-bias potentials above 60 V. The cross sections reported in this work are obtained at 80 V. The relatively low potential is chosen to maintain sufficient mass resolution to separate hydrogen-atom abstraction

products from the intense primary ion signal. The extraction electrode potentials are adjusted to maximize both secondary and primary ion count rates. Except for the highest LAB energies investigated in this work, both primary and secondary ions have equal extraction-lens settings. In the situation where this is not the case, the discrimination is accounted for by correcting for the primary beam attenuation observed when optimizing the secondary count rates.

Integral cross sections, σ, are obtained from the following expression:

$$\sigma=\frac{I_{\text{sec}}}{(I_{\text{prim}}+I_{\text{sec}})nl}, \tag{5}$$

where n is the neutral target gas density, l is the effective interaction length, I_{prim} is the transmitted primary ion beam current, and I_{sec} is the total secondary ion current. The primary and secondary ion currents are obtained by integrating the bands of a mass spectrum recorded at constant Δm conditions. Equation (5) is only valid if the target gas densities are low enough to ensure single collision conditions. This is checked by verifying that the measured cross sections are independent of the target gas density. The effective interaction length is determined using the well-known calibration reaction[22]

$$Ar^+ + D_2 \rightarrow ArD^+ + D. \tag{6}$$

Since the cross section for the reaction

$$H_2O^+ + H_2O \rightarrow H_3O^+ + OH \tag{7}$$

is very large at thermal collision energies,[23–28] very slow product H_2O^+ will produce significant amounts of H_3O^+ in secondary reactions in the collision cell. A proper charge-transfer cross section measurement must, therefore, include the H_3O^+ ion current as part of the secondary ion signal.

The main error in the reproducibility of the charge-transfer cross sections stems from the difficulty in measuring the water vapor pressure accurately. In the present apparatus, it takes ~30 min for the pressure reading to stabilize. The absolute error of the present cross-section measurements is estimated at ~30%. The relative error is considerably smaller.

The ion energy and half-width are determined by performing retardation scans of the octopole bias potential. The energy width can be substantially broadened in the octopole injection stage.[14] The broadening is minimized by injecting the primary ions as slowly as possible. The width achieved in this work is between 200 and 300 meV.

A more accurate measure of the ion energy is obtained using a TOF technique. TOF spectra are obtained by generating a pulsed ion beam with a deflector electrode situated in the injection lens, and by measuring the flight time of the primary and secondary ions using a time-to-digital converter. The primary ion energy is determined from the flight time shift observed when varying the second octopole bias potential. The uncertainty of the primary ion LAB energy scale is ±0.1 eV when determined through retardation scans, and ±0.05 eV when determined through the TOF technique.

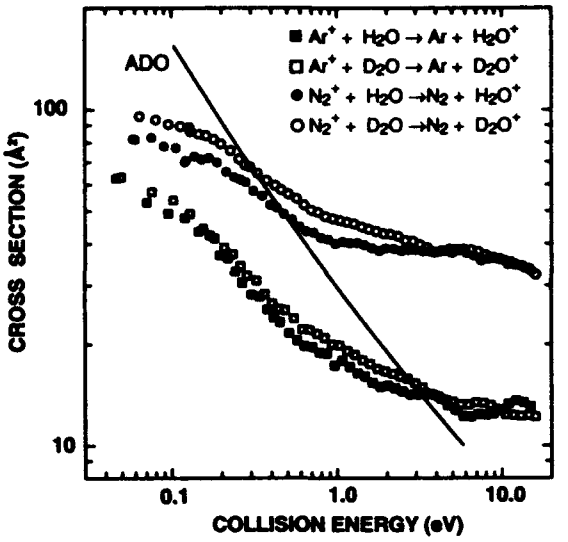

FIG. 2. Collision-energy dependence of the $Ar^+ + H_2O(D_2O)$ and $N_2^+ + H_2O(D_2O)$ charge-transfer cross sections. The cross sections are compared to ADO predictions based on the model of Bates (Refs. 30–32).

Secondary ion TOF spectra are obtained in a pulsed rf burst mode in which the rf power is briefly turned off after the expiration of the spectral time window. This purges very slow ions from the ion-guide system and therefore eliminates the background due to very slow trapped ions produced in previous TOF cycles. The raw TOF spectra are converted to velocity space using basic electrostatic equations. The TOF conversion and analysis procedure has been discussed in detail previously.[17]

III. RESULTS

A. Charge-transfer systems

The collision-energy dependence of the charge-transfer (1) and (3) cross sections is shown in Fig. 2. The GIB measurements lie ~30% below those of Turner and Rutherford,[10] and the $N_2^+ + H_2O(D_2O)$ cross sections are ~40% higher than those obtained with a thin-cell tandem-mass spectrometer.[11] The ratios between the cross sections of the two charge-transfer systems is very similar to that found by Turner and Rutherford. At low collision energies, E_T, the cross sections fall off rapidly with increasing collision energy, which is indicative of a mechanism involving complex formation. The low-energy regime has been fit to a power law, E_T^{-n}. The powers, n, are listed in Table I. The table also indicates the energy range which was fitted. The lowest energy values are omitted because they correspond to primary-ion energies below the primary beam half-width. For the charge-transfer (1) systems, n is ~0.5, the value expected from the Langevin–Gioumousis–Stevens

TABLE I. Power-fit data of low-collision energy cross sections for investigated ion-$H_2O(D_2O)$ charge-transfer reactions. n is the fit parameter of a E_T^{-n} fit. Also indicated is the collision energy range of the fit.

Reaction	n	E_T range (eV)
$Ar^+ + H_2O \rightarrow Ar + H_2O^+$	0.55	0.2–0.6
$Ar^+ + D_2O \rightarrow Ar + D_2O^+$	0.52	0.2–0.6
$N_2^+ + H_2O \rightarrow N_2 + H_2O^+$	0.39	0.2–0.7
$N_2^+ + D_2O \rightarrow N_2 + D_2O^+$	0.35	0.2–0.7

(LGS) model[29] assuming a capture mechanism involving a pure polarization potential. n is considerably lower for the charge-transfer (3) systems.

The LGS model is not accurate for the present collision systems due to the significant dipole of H_2O and the resulting ion-permanent dipole interaction. The figure also includes the average-dipole orientation (ADO) predictions based on the ADO model of Bates.[30–32] The details pertaining to the calculated curve have been discussed elsewhere.[33] At low collision energies, the model prediction comes close in absolute magnitude to the $N_2^+ + H_2O(D_2O)$ charge-transfer cross sections. Whereas the slopes of the predicted and measured energy dependencies differ in this system, they are similar in the $Ar^+ + H_2O(D_2O)$ system, for which, however, the absolute magnitude lies significantly below the model predictions. At higher energies, the cross sections become far less dependent on the collision energy than predicted by the model, exceeding the predictions in both systems. This indicates that a capture mechanism involving a longer-lived intermediate is no longer relevant at these energies, and that a direct mechanism dominates the dynamics.

At low collision energies, isotope effects are discernable in both systems. The irregular isotope effect observed at high energies for the $Ar^+ + H_2O$ system is attributed to a systematic error due to quadrupole discrimination problems stemming from the large difference in primary and product ion mass and energies.

Raw TOF spectra have been converted to product-ion velocity distributions, $f(v'_{1p})$, where v'_{1p} are product-ion LAB velocity components parallel to the octopole axis. Converted spectra recorded at four different collision energies for the $Ar^+ + H_2O$ and $N_2^+ + H_2O$ charge-transfer product ions are shown in Figs. 3 and 4, respectively. The CM velocity, v_{cm}, and that for LAB forward-scattered product ions produced in a resonant charge-transfer collision, v_{rct}, are indicated. Both velocities have been determined for a target molecule at rest. The spectra have been recorded with octopole rf amplitudes, U_0, of 100 V or higher. At some collision energies, a second spectrum is shown that was recorded at amplitudes below 30 V. Based on the expression for the effective potential in a rf octopole,[21] it is estimated that only product ions with transverse energies below 150 meV are transmitted at the low rf amplitudes.

At all of the collision energies, a main band of products with near-zero velocities and a weaker contribution of LAB-forward scattered ions with a strongly energy-dependent intensity is observed. Similar observations have been made in the $O^+ + H_2O$ system.[33,17] The cross section for the LAB forward-scattered ions, $\sigma(v'_{1p} > v_{cm})$, is obtained by determining the fraction of forward scattered signal and by measuring the charge-transfer cross section in the pulsed conditions. This cross section is lower than that obtained in a continuous mode because of the rf burst technique described in Sec. II. The energy dependence of the LAB forward-scattered cross sections is shown in Fig. 5 for the two charge-transfer systems. E_T^{-n} power fits produce values for n close to 1, which is also observed in the $O^+ + H_2O$ system. The $Ar^+ + H_2O$ data fit a $1/E_T$ dependence perfectly if the highest-energy data point is omitted. The marked energy dependence of the forward-scattered ions implies that these ions are produced in large impact parameter, orbiting collisions, rather than small impact parameter, head-on type collisions, for which a relatively weak energy dependence is expected.

Orbiting collisions involving very weakly bound complexes have been described using the osculating complex model.[15–17] This model assumes an intermediate complex with a lifetime distribution given by an exponential decay. The $O^+ + H_2O$ charge-transfer product angular distributions are found to be well characterized by an osculating complex. The solid lines in Figs. 3 and 4 are simulated distributions based on the osculating-complex model and the methodology described by Gerlich.[34] The simulations include all broadening mechanisms (i.e., thermal broadening, broadening due to collision-cell length, and primary ion pulse width). The parameters yielding the best fits of an osculating-complex model velocity distribution are shown in Tables II and III. The tables include the adjustable variables of the osculating complex model, the translational exoergicity, ΔE_T, and the complex rotational period to lifetime ratio, τ_r/τ_c. Also listed are the internal energy, $E_I = \Delta E_0 - \Delta E_T$, where ΔE_0 is the exothermicity, the angle, θ_d, signifying the direct scattering direction with respect to the primary ion LAB velocity vector, and n, the power of the cross-section energy dependence used in the model.

Except for the lowest-energy measurements, the experimental distributions are well described by a main contribution due to very large τ_r/τ_c implying a direct process, and a minor channel involving longer-lived complexes resulting in large-angle scattering. The LAB forward-scattered bands are primarily due to the longer-lived collision complexes. There is very little translational energy transfer, most of which results from longer-lived intermediates. Small amounts of efficient energy transfer appear in small-impact parameter head-on type encounters ($\theta_d = 0°$). The τ_r/τ_c of the longer-lived complexes remains approximately the same throughout the investigated collision energy range, which has also been observed for the $O^+ + H_2O$ charge-transfer system.[17]

Given the resolution of the experiment and kinematic constraints, the detection of positive translational energy transfer is only possible through the analysis of the LAB forward-scattered ions at low collision energies. The very low laboratory velocities of product ions formed in long-

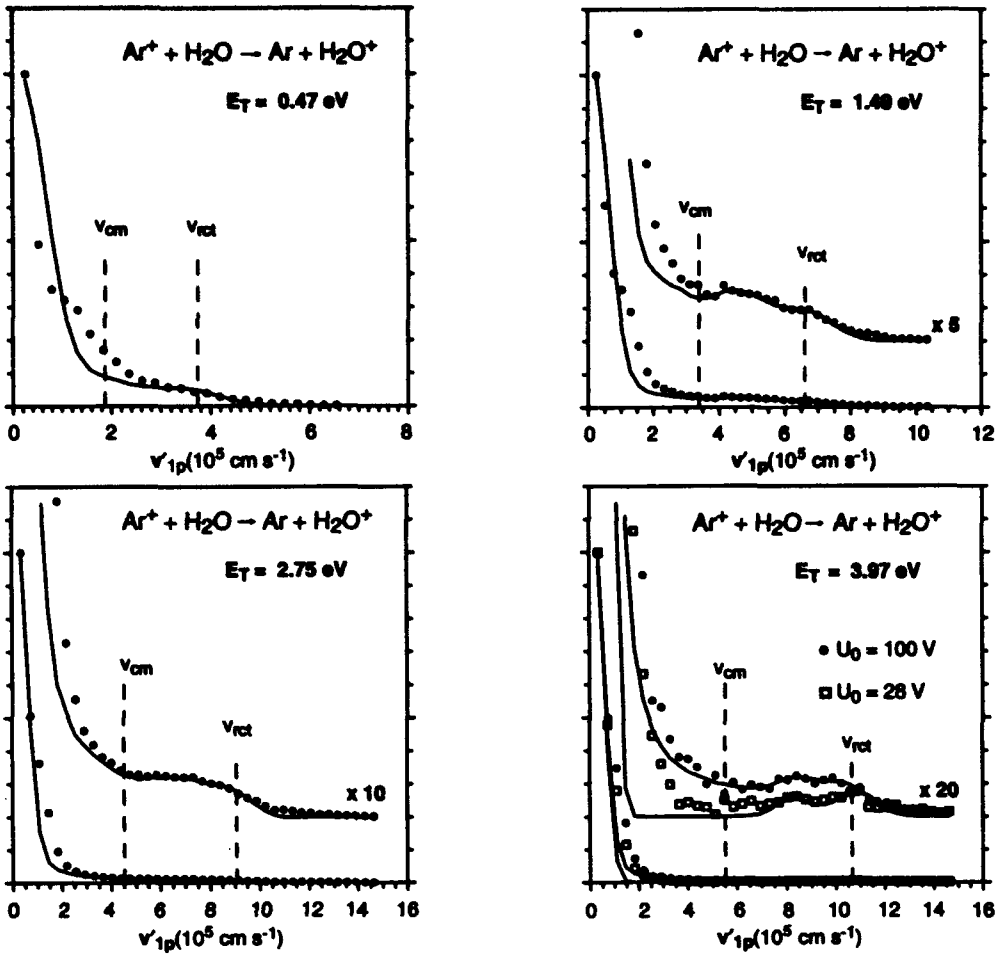

FIG. 3. Laboratory velocity distributions of $Ar^+ + H_2O$ charge-transfer product ions. All of the measurements have been recorded at an octopole rf amplitude, U_0, of 100 V or higher except where indicated. v_{cm} and v_{rct} are the center-of-mass velocities and resonant charge-transfer velocities (CM backscattered), respectively. The solid lines are numerical simulations using the formalisms described in Ref. 17. The parameters providing the best fits are shown in Table II.

range direct processes are affected by octopole-rod surface potential inhomogeneities, and therefore do not lend themselves well to studying superelastic charge transfer.

The analysis of the $Ar^+ + H_2O$ TOF data agrees well with the crossed-beam results of Glosik *et al.*[12] Those authors also found mainly near-zero translational energy transfer with a slight tendency of positive energy transfer. They also discovered evidence for H_2O^+ $\tilde{B}\,^2B_2$ state production in the CM backscattered direction ($\theta_d = 0^0$) at $E_T = 1.85$ eV. The data in Table II confirms $\tilde{B}$-state excitation, which is endothermic by 1.44 eV. Translational energy transfer exceeding 1.4 eV is observed at reactant translational energies of 1.49, 2.75, and 3.97 eV. Glosik *et al.* did not observe $\tilde{B}$-state excitation at a collision energy of 2.78 eV, which may be attributable to the lower sensitivity in the crossed-beam experiments. As in the $O^+ + H_2O$ system,[17] there is a reasonable agreement between the parameters yielding the best fit for high and low rf fields. This is demonstrated in Table II for $E_T = 3.97$ eV. The osculating complex, therefore, provides an adequate description of the angular distributions. This is not surprising considering the long-range nature of the interaction, implying a simple angular scattering pattern governed by classical collision dynamics.

The translational energy transfer distributions are similar in the $N_2^+ + H_2O$ charge-transfer system. As seen in Table III, the lifetimes of the longer-lived complexes are somewhat longer compared with the $Ar^+ + H_2O$ system. The $\tilde{B}$ state, which is endothermic by 1.62 eV, also appears to be accessed in this system in small-impact parameter collisions. The low-guiding-field simulations shown in Fig. 4 for $E_T = 1.96$ and 4.25 eV are based on the same translational energy transfer and complex-lifetime distributions yielding the best fit for the high-field distributions. The osculating-complex model, therefore, also provides a good description of the angular distributions in this system.

The measurement at $E_T = 11.7$ eV exhibits strongly superelastically scattered ions. Due to the very weak signal associated with these ions, this result must be treated with caution. It is possible that this signal originates from imperfect primary-ion holdoff in the deflector electrode.

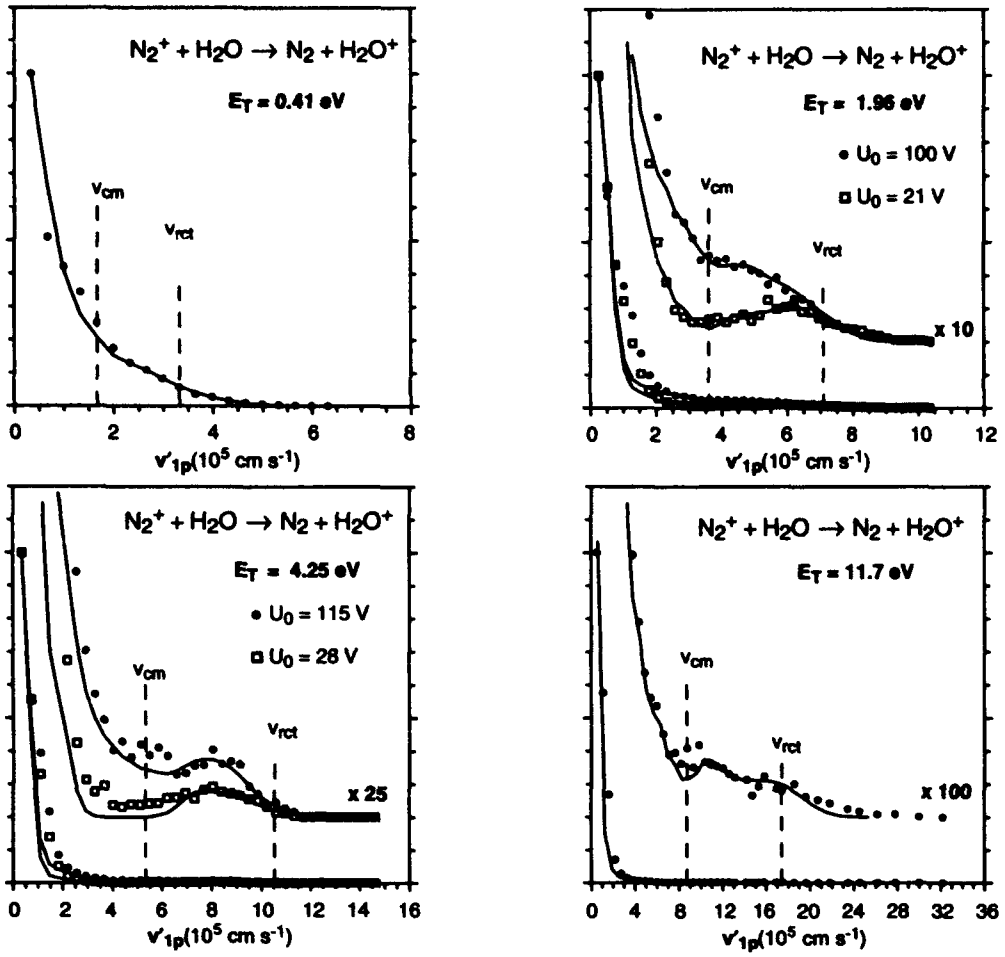

FIG. 4. Laboratory velocity distributions of $N_2^+ + H_2O$ charge-transfer product ions. All of the measurements have been recorded at an octopole rf amplitude, U_0, of 100 V or higher except where indicated. v_{cm} and v_{rct} are the center-of-mass velocities and resonant charge-transfer velocities (CM backscattered), respectively. The solid lines are numerical simulations using the formalisms described in Ref. 17. The parameters providing the best fits are shown in Table III.

B. Atom-abstraction channel

The energy dependence of the atom-abstraction cross sections for the $Ar^+ + H_2O(D_2O)$ and $N_2^+ + H_2O(D_2O)$ collision systems are shown in Figs. 6 and 7, respectively. Also included in the figure are the total cross sections consisting of the sum of atom-abstraction and charge-transfer cross sections. The measurements of reaction (2) are the first hyperthermal cross sections of this system known to us. The GIB measurements of reaction (4) are approximately a factor of 2 higher than those determined in a thin-cell tandem-mass spectrometer,[11] indicating that collection was inefficient in that experiment. The atom-abstraction cross sections decline rapidly with collision energy at low energies, then become fairly independent of energy, before declining again. The atom-abstraction reaction (4) exhibits a significantly higher cross section than that of reaction (2). The ratios between atom-transfer and charge-transfer cross sections are, however, comparable for the two systems. Low-energy power fits have been carried out for the atom-abstraction reactions, as for the charge-transfer systems. The best power-law fits are listed in Table

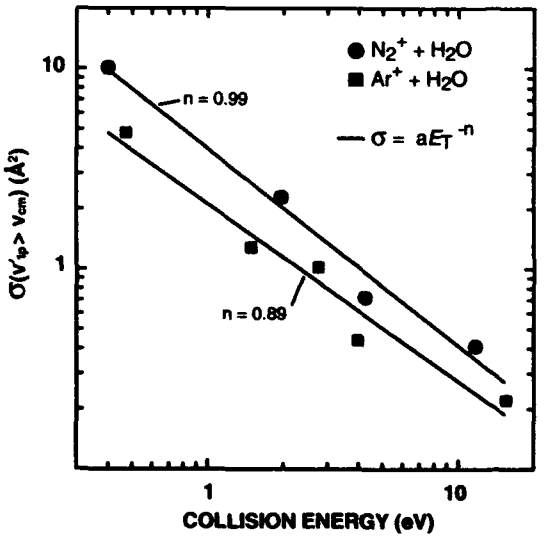

FIG. 5. Collision-energy dependence of the LAB forward-scattered cross sections for the $Ar^+ + H_2O$ and $N_2^+ + H_2O$ charge-transfer product ions. The experimental data are fit to a power law aE_T^{-n}.

TABLE II. Simulation parameters for $Ar^+ + H_2O$ charge transfer TOF spectra. U_0 is the rf amplitude applied to the octopole, c are the statistical weights of the distributions $S(v'_{i\rho};\Delta E_T,\tau_r/\tau_c)$, ΔE_T is the translational exoergicity, E_I is the product internal energy assuming Ar^+ ($^2P_{3/2}$) reactant ions, τ_r/τ_c is the complex rotational period-to-complex lifetime ratio, n is the cross section power dependence, and θ_d is the direct scattering angle with respect to the primary ion velocity vector.

E_T (eV)	U_0 (V)	c	ΔE_T (eV)	E_I (eV)	τ_r/τ_c	n	θ_d
0.47	100	0.44	0	3.14	1	0.5	180°
		0.17	0.2	2.94	12	0.5	180°
		0.20	0.2	2.94	7	0.5	180°
		0.20	0.4	2.74	7	0.5	180°
1.49	100	0.58	0	3.14	30	0	180°
		0.006	−1.0	4.14	30	0	0°
		0.005	−1.4	4.54	30	0	0°
		0.004	−1.49	4.63	30	0	0°
		0.077	0.2	2.94	7	0	180°
		0.090	0.4	2.74	7	0	180°
		0.236	0.6	2.54	7	0	180°
2.75	100	0.64	0	3.14	30	0	180°
		0.003	−1.5	4.64	30	0	0°
		0.003	−2.0	5.14	30	0	0°
		0.003	−2.5	5.64	30	0	0°
		0.232	0.2	2.94	7.5	0	180°
		0.120	0.4	2.74	7.5	0	180°
3.97	100	0.89	0	3.14	30	0	180°
		0.002	−2.5	5.64	30	0	0°
		0.002	−3.0	6.14	30	0	0°
		0.110	0	3.14	5	0	180°
	29	0.89	0	3.14	30	0	180°
		0.003	−2.5	5.64	30	0	0°
		0.006	−3.0	6.14	30	0	0°
		0.097	0	3.14	5	0	180°

IV. The n values are considerably larger than those for the charge-transfer systems, indicating that a longer interaction time favors these reactions.

Whereas the total cross section of the $Ar^+ + H_2O(D_2O)$ collision system lies substantially below the ADO predictions at low collision energies, the measured total cross sections of the $N_2^+ + H_2O(D_2O)$ collision system coincide with the model prediction at the lowest meaningful collision energies of this experiment. The logarithmically plotted data has a substantially smaller slope, however, suggesting that a direct mechanism is prominent throughout the measured collision energy range.

Both atom-abstraction reaction systems exhibit a distinct isotope effect in which hydrogen-atom abstraction is more efficient than deuterium-atom abstraction. Within the experimental uncertainties, no isotope effect is observed in the total cross sections. The isotope effects observed in the charge-transfer systems can thus be rationalized as stemming from competition between charge transfer and atom abstraction.

The isotope effect can be explained using the simple kinematic *spectator-stripping*[35–39] or the more general *pairwise-energy* models.[40] In these models, the reaction is regarded to occur solely between the reactant ion and the transferred atom while the product neutral moiety is postulated to remain unaffected throughout the collision. In such association reactions, no isotope effect is expected if only kinematic arguments are considered. The atom-abstraction isotope effect is, thus, expected to disappear if the cross sections are plotted with respect to the pairwise energy, E_{pair}, consisting of the energy absorbed in the pairwise association reaction

$$E_{pair} = (1 - m_1/m_1')E_{lab}, \tag{8}$$

where m_1 is the primary-ion mass, m_1' is the product-ion mass, and E_{lab} is the primary-ion LAB energy. The atom-abstraction cross sections for reactions (2) and (4) are shown on a pairwise-energy scale in Figs. 8 and 9. Except for the hyperthermal energy regime of reaction (2), an isotope effect is no longer visible within the experimental error. The error for the $Ar^+ + H_2O$ atom-transfer measurements is considerably higher than for the deuterated reaction due to the overlapping signals of the $m/e = 40$ and 41 bands. It can, therefore, be maintained that the difference between the isotopic cross sections at hyperthermal energies where the cross sections are small is within experimental error.

The rapid decline of the atom-transfer cross sections with collision energy at collision energies of ~10 eV may be attributed to dissociation of the product ions. Within the spectator-stripping model, a sudden loss of product-ion signal would be expected at the pairwise energy equal to the proton affinity of Ar and N_2 minus the respective reaction enthalpy. In the $Ar^+ + D_2O$ system, the onset for the decline is at $E_{pair} = 1$ eV, considerably lower than pairwise dissociation onset of 2.9 eV,[41] while in the $N_2^+ + H_2O(D_2O)$ atom-abstraction reactions, an onset of ~0.6 eV is observed, which is also considerably below the pairwise onset of 3.2 eV.[41] Product dissociation is, there-

TABLE III. Simulation parameters for $N_2^+ + H_2O$ charge transfer TOF spectra. U_0 is the rf amplitude applied to the octopole, c are the statistical weights of the distributions $S(v'_{1p};\Delta E_T,\tau_r/\tau_c)$, ΔE_T is the translational exoergicity, E_T is the product internal energy assuming ground state reactants, τ_r/τ_c is the complex rotational period-to-complex lifetime ratio, n is the cross section power dependence, and θ_d is the direct scattering angle with respect to the primary ion velocity vector.

E_T (eV)	U_0 (V)	c	ΔE_T (eV)	E_I (eV)	τ_r/τ_c	n	θ_d
0.41	100	0.420	0	2.96	20	0.5	180°
		0.287	0	2.96	12.5	0.5	180°
		0.046	0.6	2.36	4	0.5	180°
		0.051	0.4	2.56	4	0.5	180°
		0.055	0.2	2.76	4	0.5	180°
		0.074	0	2.96	4	0.5	180°
		0.111	−0.2	3.16	4	0.5	180°
		0.080	−0.4	3.36	4	0.5	180°
1.96	100	0.893	0	2.96	30	0	180°
		0.003	−1.8	4.76	30	0	0°
		0.002	−2.0	4.96	30	0	0°
		0.055	0.4	2.56	5	0	180°
		0.038	0.2	2.76	5	0	180°
		0	0	2.96	5	0	180°
		0.024	−0.4	3.36	5	0	180°
		0.073	−0.8	3.76	5	0	180°
		0.032	−1.2	4.16	5	0	180°
		0.032	−1.6	4.56	5	0	180°
4.25	115	0.900	0	2.96	30	0	180°
		0.029	0	2.96	5	0	180°
		0.059	−2.0	5.96	5	0	180°
		0.002	−3.2	6.16	30	0	0°
		0.002	−3.6	6.56	30	0	0°
11.7	115	0.904	0	2.96	30	0	180°
		0.092	2.9	5.86	7.5	0	180°
		0.001	−11.5	14.46	30	0	0°

fore, a with respect to the spectator-stripping model inconsistent explanation for the cross-section drop.

The spectator-stripping model has important implications regarding the product velocity distributions. According to this model, the product ions are formed with LAB velocities equal to the CM velocity of the primary-ion–abstracted-atom system. Applying conservation of momentum, and assuming a target molecule at rest, the product-ion LAB velocity, v'_1, is then given by

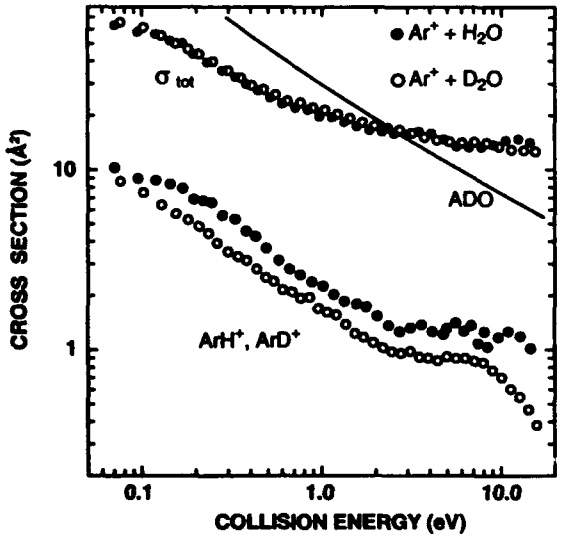

FIG. 6. Energy dependence of the $Ar^+ + H_2O(D_2O)$ atom abstraction reaction cross sections. Also shown are the respective total cross sections including charge transfer and atom abstraction and the ADO predictions using the model of Bates (Refs. 30–32).

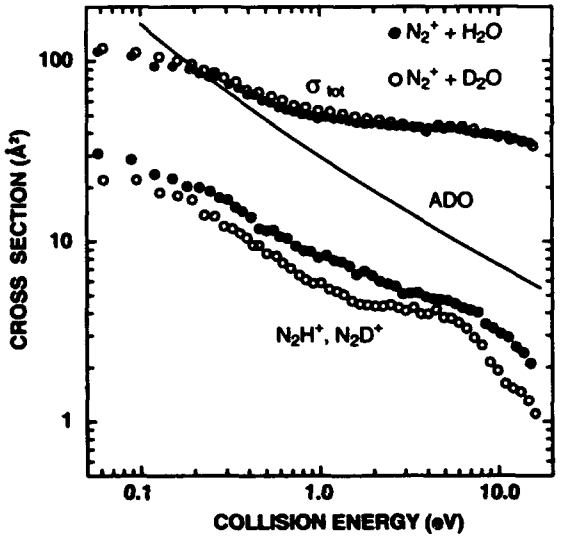

FIG. 7. Energy dependence of the $N_2^+ + H_2O(D_2O)$ atom abstraction reaction cross sections. Also shown are the respective total cross sections including charge transfer and atom abstraction and the ADO predictions using the model of Bates (Refs. 30–32).

TABLE IV. Power-fit data of low-collision energy cross sections for investigated ion-$H_2O(D_2O)$ atom-abstraction reactions. n is the fit parameter of a E_T^{-n} fit. Also indicated is the collision energy range of the fit.

Reaction	n	E_T range (eV)
$Ar^+ + H_2O \rightarrow ArH^+ + OH$	0.68	0.2–2
$Ar^+ + D_2O \rightarrow ArD^+ + OD$	0.64	0.2–2
$N_2^+ + H_2O \rightarrow N_2H^+ + OH$	0.52	0.2–2
$N_2^+ + D_2O \rightarrow N_2D^+ + OD$	0.64	0.2–1

$$v_1' = \frac{m_1}{m_1^*} v_1. \tag{9}$$

Equation (9) predicts product to primary-ion LAB velocities of 0.952 and 0.933 for reactions (2) and (4), respectively. TOF measurements have been conducted for the deuterated systems over a broad range of energies. Figures 10 and 11 are examples of ArD^+ and N_2D^+ TOF spectra taken at $E_T = 10$ and 5 eV, respectively. The solid lines are simulations assuming a direct process ($\tau_r/\tau_c \gg 1$) and $\Delta E_T = -E_{pair}$. In both cases, the maxima of the calculated curves agree very well with the experimental data, which are slightly broader than the model predictions indicating a broadened product internal-energy distribution. The asymmetry in the N_2D^+ velocity distributions can be related to a slightly asymmetric primary ion velocity distribution that is probably due to imperfect injection of ions into the octopole system.

The product to primary ion LAB velocity ratios, v'_{1pmax}/v_{1pmax}, determined from the maxima of the velocity-transformed TOF spectra for the two atom-abstraction reactions, are listed in Tables V and VI. Except for the lowest energy measurements, the ratios agree well with the spectator-stripping predictions given by Eq. (9). The lowest-energy measurements exhibit significant angular scattering, which could account for a shift of the velocity distribution maxima at lower values. This conclusion is supported by low-energy higher resolution crossed-beam measurements of reaction (2), which are in very good agreement with spectator-stripping predictions.[12]

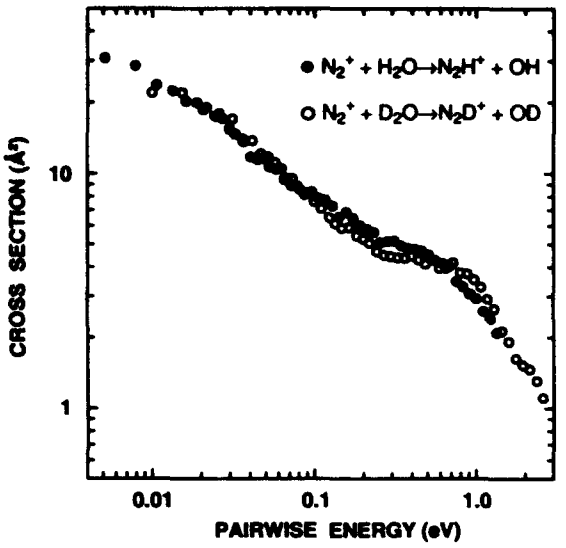

FIG. 9. Pairwise-energy dependence of the $N_2^+ + H_2O(D_2O)$ atom abstraction reaction cross section.

IV. DISCUSSION

A. Charge-transfer systems

In the past it has been shown that the magnitude of state-to-state ion–molecule charge-transfer cross sections is generally governed by two criteria, energy resonance between the reactants and products, and Franck–Condon overlap.[7,8,42–44] A large state-to-state cross section thus re-

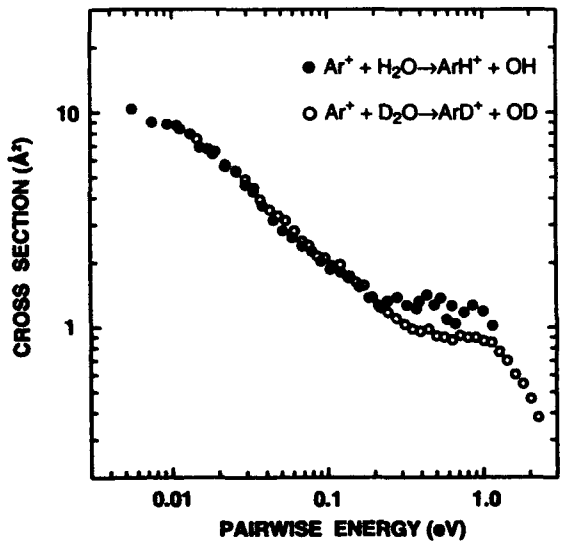

FIG. 8. Pairwise-energy dependence of the $Ar^+ + H_2O(D_2O)$ atom-abstraction reaction cross section.

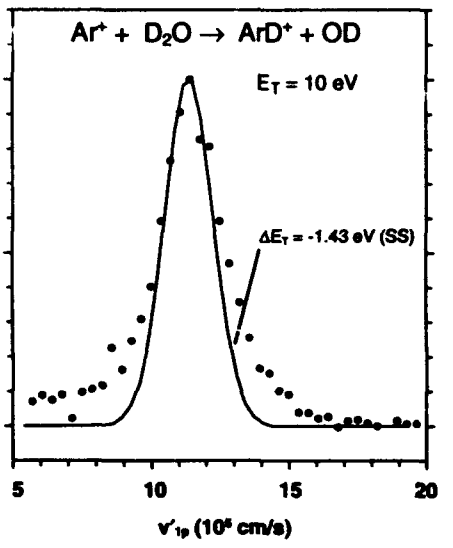

FIG. 10. Laboratory velocity distributions of $Ar^+ + D_2O$ atom-abstraction product ions, ArD^+, at $E_T = 10$ eV. The solid line is a simulation assuming translational energy transfer corresponding to the spectator-stripping model, i.e., $\Delta E_T = -E_{pair}$.

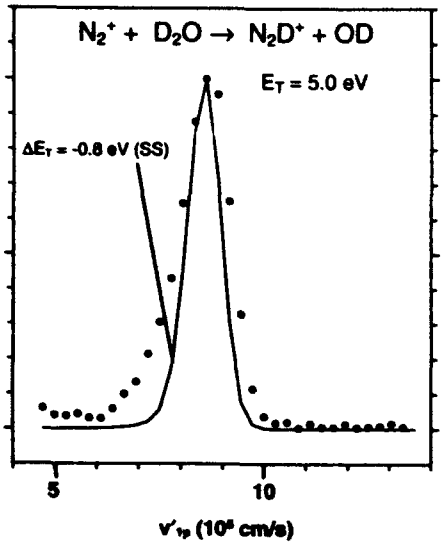

FIG. 11. Laboratory velocity distributions of $N_2^+ + D_2O$ atom-abstraction product ions, N_2D^+, at $E_T = 5$ eV. The solid line is a simulation assuming a translational energy transfer corresponding to the spectator-stripping model, i.e., $\Delta E_T = -E_{pair}$.

quires a significant Franck–Condon overlap between the reactant and product vibrational wavefunctions as well as a small energy gap at infinite intermolecular distances. These criteria follow from semiclassical models of nonadiabatic transitions, which are governed by the magnitude of the vibronic coupling between the reactant and product states.[42–45] Energy-resonance and Franck–Condon arguments predict product energy distributions that contrast those associated with long-lived complexes where a statistical energy distribution is assumed. Long-range interactions involving nonadiabatic transitions have limited the success of statistical theories such as phase space theory[46–48] in reproducing thermal charge-transfer rate constants.

The influence of longer-lived intermediate collision complexes on the magnitude of ion–molecule reaction cross sections can be evaluated by comparing the energy dependence of gas-phase ion–molecule cross sections to the capture cross section given by the long-range interaction (LGS capture cross section), or to extensions of this model such as the ADO model[30–32,49–52] that include the ion-permanent-dipole interaction. In the presently discussed

TABLE V. Ratios $v'_{1p\,max}/v_{1p\,max}$ between maxima of primary ion and product ion velocity distributions of the reaction $Ar^+ + D_2O \rightarrow ArD^+ + OD$. The spectator stripping prediction is 0.952.

E_T (eV)	$v'_{1p\,max}/v_{1p\,max}$
0.57	0.894±0.040
0.83	0.939±0.035
1.33	0.938±0.030
2.67	0.923±0.030
6.00	0.938±0.020
10.0	0.948±0.023
13.3	0.964±0.027

TABLE VI. Ratios $v'_{1p\,max}/v_{1p\,max}$ between maxima of primary ion and product ion velocity distributions of the reaction $N_2^+ + D_2O \rightarrow N_2H^+ + OD$. The spectator stripping prediction is 0.933.

E_T (eV)	$v'_{1p\,max}/v_{1p\,max}$
1.00	0.917±0.040
2.04	0.954±0.032
3.33	0.935±0.025
4.17	0.926±0.022
5.00	0.944±0.029
5.83	0.965±0.025
6.67	0.945±0.021
10.3	0.940±0.023
12.5	0.918±0.024

systems, it is appropriate to compare the models with the total reaction cross sections, since we have two significant product channels. The agreement between ADO predictions and the $N_2^+ + H_2O(D_2O)$ total cross section is good at the lowest meaningful energy of this work. The experimental data, however, fall off less steeply than the model predicts, indicating that a direct mechanism is highly efficient at very low collision energies. This is clearly corroborated by the lowest-energy TOF measurement at $E_T = 0.41$ eV, where more than 70% of the product ions are found to be produced in collisions with $\tau_r/\tau_c > 10$.

The $Ar^+ + H_2O(D_2O)$ total cross section on the other hand is much smaller in magnitude than the ADO prediction. The slope of the low-energy logarithmic energy dependence, however, agrees quite well with the ADO predictions. This suggests that a direct mechanism is considerably less efficient in this charge-transfer system, and that capture collisions overcome the constraints to a certain degree.

The large cross sections observed for charge-transfer (3) indicate efficient near-resonant state-to-state cross sections in very large impact parameter collisions. This is confirmed by the TOF analysis shown in Table III, where the majority of product ions are found to be produced within a small band about resonance. The large state-to-state cross sections near resonance are also consistent with significant bending vibrational Franck–Condon factors of the $\tilde{A}\,^2A_1$ state (seen in the photoelectron spectrum of H_2O)[53,54] for collisions involving only internal excitation of the H_2O^+ moiety. The TOF data are in good agreement with the analysis of charge-transfer luminescence measurements,[6] showing that H_2O^+ $\tilde{A}$-state bending vibrational levels close to resonance are populated in the charge-transfer collisions.

The fact that the $Ar^+ + H_2O(D_2O)$ charge-transfer product TOF data are similar to those observed in charge-transfer (3) indicates that the smaller charge-transfer cross sections observed in this system are due to a weaker vibronic coupling near resonance. The TOF as well as the charge-transfer luminescence measurements[6] demonstrate an equally strong preference for near-resonant product ion population. In the luminescence measurements, it is found that energy resonance only applies to $Ar^+(^2P_{3/2})$ ions because no emissions are observed for H_2O^+ levels resonant

with the $^2P_{1/2}$ spin–orbit state, which is populated by ~30% of the primary ions. This is a strong indication that the $Ar^+(^2P_{1/2}) + H_2O$ charge-transfer cross section is significantly smaller than that of $Ar^+(^2P_{3/2}) + H_2O$, and that the latter is therefore ~50% higher than the experimental data shown in Fig. 2. The thus corrected $^2P_{3/2}$ cross section is still considerably smaller than that of charge-transfer (3). The smaller difference can now, however, be rationalized by the smaller Franck–Condon factors of H_2O ionization at resonance with $Ar^+(^2P_{3/2})$ compared to those experienced during resonant $N_2^+(X\,^2\Sigma_g^+) - N_2(X\,^2\Sigma_g^+)\Delta v = 0$ charge-transfer transitions. It may be argued that the different size of the primary ions could affect the total cross section. The large cross sections of charge-transfer (3), as well as those observed for the $O^+ + H_2O$ charge transfer,[33] however, demonstrate that these hyperthermal charge-transfer reactions proceed at average intermolecular distances exceeding 4 Å. At such intermolecular distances, it is doubtful that the difference in Ar^+ and N_2^+ primary ion size plays a role.

At all of the collision energies at which TOF measurements have been conducted, the energy distributions are highly nonstatistical. This is consistent with the very short complex lifetimes found to provide an adequate fit of the data. Since most of the complexes do not survive one rotational period, the LAB forward-scattered signal is representative of the longest-lived collision complexes. As seen in Fig. 5, the energy dependence of the intensity of LAB forward-scattered ions exhibits a $1/E_T$ dependence for the $N_2^+ + H_2O(D_2O)$ system and implies that the ion–dipole interaction plays a key role in the longest-lived collision complexes. The latter conclusion stems from the $1/E_T$ energy dependence of the capture cross section of a pure ion–dipole interaction. The $Ar^+ + H_2O(D_2O)$ LAB forward-scattered energy dependence fits a $1/E_T$ dependence exactly if the highest-energy data point is omitted. That data point includes considerable contributions due to small-impact parameter hard-sphere type scattering, as seen in Table II, thus raising the forward-scattered signal above the levels expected for pure orbiting collisions. It is, therefore, concluded that the longest-lived complexes are formed in those collisions where the dipole is optimally oriented to provide the strongest attraction. Identical observations are made for the $O^+ + H_2O$ charge-transfer system,[33] further validating the experimental results.

In both presently discussed systems, as well as in the $O^+ + H_2O$ charge-transfer reaction, the complex rotational period-to-complex lifetime ratio of the longer-lived contribution remains fairly constant throughout the investigated collision energy range. Since the average impact parameters may be assumed relatively independent of collision energy for a direct mechanism, the experimental results indicate that the average complex lifetime of the longest-lived intermediates decreases with collision energy. This is reflected by the higher degree of energy randomization at lower collision energies. The charge-transfer (3) lifetimes are somewhat longer than those of charge-transfer (1), which may be explained by the stronger product long-range interaction of the former. The most relevant finding regarding the complex lifetimes is certainly that no contributions of long-lived complexes, i.e., $\tau_r/\tau_c < 1$, are found down to collision energies of 0.40 eV. This may be explained by the extremely large average intermolecular distances at which the electron hop occurs, and the very weak interaction potentials, especially those of the products, at these intermolecular distances. In other words, the average impact parameters leading to charge transfer are significantly larger than those leading to long-lived complexes. The reason why smaller-impact parameter collisions are not more noticeable in the product velocity distributions may be related to competition with the atom-abstraction channel once regions of the chemical potential are probed.

B. Atom-abstraction reactions

As shown in Sec. III B, the spectator-stripping or pairwise energy models can account for the observed isotope effects as well as product-ion velocity distributions. In both systems, there is a relatively sharp decline in cross section at hyperthermal collision energies. Within the framework of the pairwise-energy model this decline cannot be related to the dissociation of the product ions because the onset lies significantly below the pairwise-energy threshold.

The relatively strict adherence to the pairwise-energy model implies that the pairwise-energy dependence of these systems should be similar to those of the $Ar^+ + H_2(D_2)$ and $N_2^+ + H_2(D_2)$ atom-abstraction reactions. Armentrout and co-workers[22,55] have studied those systems and find that the cross sections do in fact exhibit a decrease in the slope of the logarithmically plotted data at similar pairwise energies, followed by the onset of a steeper decline at the respective pairwise dissociation energy. The weak onset was explained with an enhancement of nonreactive trajectories at higher relative translational energies.

The presently studied H_2O systems differ from the H_2 reactions because of the highly efficient charge-transfer channel. The observation of high rotational excitation of the chemiluminescent neutral atom-abstraction product, OH, is rationalized to originate form bending vibrational angular momentum of the intermediate $H_2O^+ A\,^2A_1$ state,[9] and thus presents evidence that the atom-abstraction reactions proceed preferentially via the charge-transfer surface involving proton transfer in a two-step process. This assertion is further bolstered by the finding that proton transfer is approximately an order of magnitude more efficient than atom abstraction in reaction (7).[23] The atom-abstraction cross section is, therefore, in part controlled by the charge-transfer cross section, which is fairly energy independent at hyperthermal energies. This may explain why the atom-abstraction cross sections level off at hyperthermal energies before declining due to possible competition with nonreactive charge-transfer channels.

The onset of OH chemiluminescence does not strictly adhere to pairwise-energy predictions assuming energy uptake by the spectator, OH. The thresholds for OH chemiluminescence are 3.1 and 2.1 eV for reactions (2) and (4), respectively. The observed chemiluminescence onsets are 11.5 and 5.9 eV, and lie significantly below the respective pairwise-energy predicted onsets of 22 and 13 eV, respec-

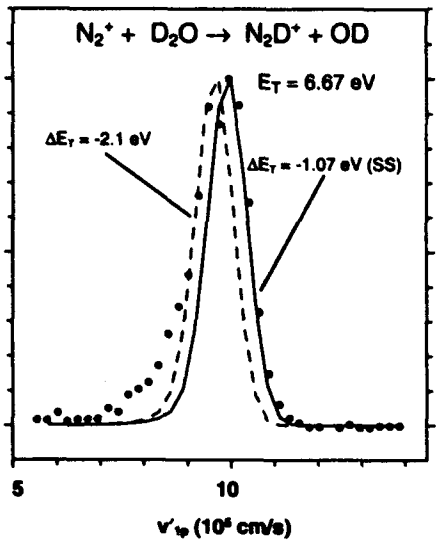

FIG. 12. Laboratory velocity distributions of $N_2^+ + D_2O$ atom abstraction product ions, N_2D^+, at $E_T = 10$ eV. The solid line is a simulation assuming a translational energy transfer corresponding to the spectator stripping model, i.e., $\Delta E_T = -E_{pair}$. The dashed line is obtained for $\Delta E_T = -2.1$ eV, corresponding to the energy transfer necessary for OH $A\,^2\Sigma^+$ population.

tively. The TOF measurements indicate that the internal energy distribution of atom-abstraction reaction products is relatively broad and centered at the spectator-stripping prediction. The estimated cross sections for OH A-state production[9] are considerably smaller than the total atom-abstraction cross sections, and consistent with the observed chemiluminescence representing the high-internal energy tail of the product internal-energy distribution. This is demonstrated in Fig. 12, where an N_2D^+ TOF spectrum is shown that is recorded at a reactant translational energy of 6.67 eV which exceeds the OH chemiluminescence onset of 5.9 eV. The spectrum is compared to the velocity distribution expected in a spectator-stripping model. Broadening towards smaller LAB velocities indicating higher internal excitation is clearly observed and is significantly less evident at $E_T = 5$ eV. A simulation representing a translational energy transfer of 2.1 eV, the threshold for OH A-state formation, is shown with a dashed line. The simulation clearly demonstrates that the chemiluminescence onset is consistent with the TOF measurements.

V. CONCLUSIONS

The $Ar^+ + H_2O(D_2O)$ and $N_2^+ + H_2O(D_2O)$ charge-transfer systems are characterized by the long-range nature of the interaction. The $N_2^+ + H_2O(D_2O)$ charge-transfer cross section is significantly larger than the $Ar^+ + H_2O(D_2O)$ cross section. The difference can be explained by the lower resonant Franck–Condon factors of charge-transfer system (1). Franck–Condon factor arguments imply that the $Ar^+(^2P_{1/2})$ spin–orbit state is practically nonreactive. This is consistent with H_2O^+ $A\,^2A_1$–$\tilde{X}\,^2B_1$ luminescence measurements in which resonant charge-transfer from the excited spin–orbit state is not observed.[6] The TOF measurements exhibit primarily near-resonant product internal excitation, in further agreement with the luminescence measurements. Small contributions due to orbiting collisions are observed. The $1/E_T$ dependence of the orbiting collision intensity is interpreted as evidence that these collisions are due to dipole orientations in which the long-range attractive forces are maximized. Osculating complex simulations indicate that the lifetimes of the longest-lived collision complexes are considerably shorter than a rotational period. This is reflected by the small amount of energy randomization observed for the longer-lived complexes. Smaller impact parameter collisions are found to lead to H_2O^+ B-state excitation, in agreement with crossed-beam observations of charge-transfer (1).[12]

The charge-transfer cross sections exhibit a weak isotope effect that can be related to competition with the atom-abstraction channels. The atom-abstraction reactions are found to be governed by a pairwise-energy mechanism and thus feature significant isotope effects that disappear once the isotopic cross sections are plotted on a pairwise-energy scale. The TOF analysis shows product ion velocity distributions that are centered at the spectator-stripping prediction, but exhibit significant broadening that is related to a broad product internal-energy distribution. The broadening can account for the discrepancy between the observed OH $A\,^2\Sigma^+$–$X\,^2\Pi$ chemiluminescence onset[9] and that predicted by a pairwise-energy model in which the spectator absorbs the excess energy.

ACKNOWLEDGMENTS

The authors thank J. A. Gardner for his support during the construction of the GIB apparatus and for helpful discussions. The authors are particularly indebted to D. Gerlich and S. L. Anderson for their invaluable assistance in designing the experiment. This work is supported by AFOSR under Task 2303EP2.

[1] J. S. Picket, G. R. Murphy, W. S. Kurth, C. K. Goertz, and S. D. Shawan, J. Chem. Phys. A **90**, 3487 (1985).
[2] E. Wulf, and U. von Zahn, J. Geophys. Res. **90**, 3270 (1986).
[3] R. A. Dressler, J. A. Gardner, D. L. Cooke, and E. Murad, J. Geophys. Res. **96**, 13 795 (1992).
[4] R. A. Dressler and E. Murad, in *Current Topics in Ion Chemistry and Ion Physics*, edited by C. Y. Ng (CRC, 1993), Vol. III.
[5] R. A. Dressler, J. A. Gardner, R. L. Lishawa, R. H. Salter, and E. Murad, J. Chem. Phys. **93**, 9189 (1990).
[6] Rainer A. Dressler, J. A. Gardner, R. H. Salter, and E. Murad, J. Chem. Phys. **96**, 1062 (1992).
[7] E. A. Gislason and G. Parlant, Comments At. Mol. Phys. **19**, 157 (1987).
[8] J. B. Laudenslager, W. T. Huntress, Jr., and M. T. Bowers, J. Chem. Phys. **61**, 4600 (1974).
[9] J. A. Gardner, R. A. Dressler, R. H. Salter, and E. Murad, J. Chem. Phys. **97**, 2473 (1992).
[10] B. R. Turner and J. A. Rutherford, J. Geophys. Res. **73**, 6751 (1968).
[11] R. A. Dressler, J. A. Gardner, R. H. Salter, F. J. Wodarczyk, and E. Murad, J. Chem. Phys. **92**, 1117 (1990).
[12] J. Glosik, B. Friedrich, and Z. Herman, Chem. Phys. **60**, 369 (1981).
[13] E. Teloy and D. Gerlich, Chem. Phys. **4**, 417 (1974).
[14] D. Gerlich, Adv. Chem. Phys. **82**, Part 1, p. 1 (1992).
[15] G. A. Fisk, J. D. McDonald, and D. R. Herschbach, Discuss. Faraday Soc. **44**, 228 (1967) (communication).

[16] M. K. Bullit, C. H. Fisher, and J. L. Kinsey, J. Chem. Phys. **60**, 478 (1974).
[17] R. A. Dressler, R. H. Salter, and E. Murad, Chem. Phys. Lett. **204**, 111 (1993).
[18] G. Henri, M. Lavollee, O. Dutuit, J. B. Ozenne, P. M. Guyon, and E. A. Gislason, J. Chem. Phys. **88**, 6381 (1988).
[19] S. Scherbarth and D. Gerlich, J. Chem. Phys. **90**, 1610 (1989).
[20] D. Gerlich, R. Disch, and S. Scherbarth, J. Chem. Phys. **87**, 350 (1987).
[21] D. Gerlich, in *Electronic and Atomic Collisions*, edited by D. C. Lorents, W. E. Meyerhof, and J. R. Peterson (Elsevier, New York, 1986), pp. 541–553.
[22] K. M. Ervin and P. B. Armentrout, J. Chem. Phys. **83**, 166 (1985).
[23] C. R. Lishawa, R. A. Dressler, J. A. Gardner, R. H. Slater, and E. Murad, J. Chem. Phys. **93**, 3196 (1990).
[24] R. A. Fluegge, J. Chem. Phys. **50**, 4373 (1969).
[25] A. Good, D. A. Durden, and P. Kebarle, J. Chem. Phys. **52**, 212 (1970).
[26] R. C. Bolden and N. D. Twiddy, Faraday Discuss. Chem. Soc. **53**, 192 (1972).
[27] W. T. Huntress and R. F. Pinizzotto, J. Chem. Phys. **59**, 4742 (1973).
[28] J. Sunner and I. Szabo, Int. J. Mass Spectrosc. Ion Phys. **31**, 213 (1979).
[29] G. Gioumousis and D. P. Stevens, J. Chem. Phys. **29**, 292 (1958).
[30] D. R. Bates, Chem. Phys. Lett. **82**, 396 (1981).
[31] D. R. Bates, Proc. R. Soc. London, Ser. A **384**, 289 (1982).
[32] D. R. Bates, Chem. Phys. Lett. **111**, 428 (1984).
[33] R. A. Dressler, R. H. Salter, and E. Murad, Planet. Space Sci. **40**, 1695 (1992).
[34] D. Gerlich, J. Chem. Phys. **90**, 1[illegible]1989).
[35] A. Henglein and K. Lacmann, Adv. Mass Spectrom. **3**, 331 (1966).
[36] K. Lacmann and A. Henglein, Phys. Chem. Ber. Berlin Bunsenges. Phys. Chem. **69**, 292 (1965).
[37] A. Ding, K. Lacmann, and A. Henglein, Ber. Berlin Bunsenges. Phys. Chem. **71**, 596 (1967).
[38] Z. Herman, J. Kerstetter, T. Rose, and R. Wolfgang, Discuss. Faraday Soc. **44**, 123 (1967).
[39] W. R. Gentry, E. A. Gislason, Y. T. Lee, B. H. Mahan, and C. W. Tsao, Discuss. Faraday Soc. **44**, 137 (1967).
[40] J. L. Elkind and P. B. Armentrout, J. Chem. Phys. **84**, 4862 (1986).
[41] S. G. Lias, J. E. Bartmess, J. F. Liebman, J. L. Holmes, R. D. Levin, and W. G. Mallard, J. Phys. Chem. Ref. Data **17**, Suppl. 1, 1 (1989).
[42] E. A. Gislason, G. Parlant, and M. Sizun, Adv. Chem. Phys. **82**, Part 2, p. 321 (1992).
[43] M. R. Spalburg, J. Los, and E. A. Gislason, Chem. Phys. **94**, 327 (1985).
[44] H. Nakamura, Adv. Chem. Phys. **82**, 243 (1992).
[45] E. Bauer, E. R. Fisher, and G. R. Gilmore, J. Chem. Phys. **51**, 4173 (1969).
[46] J. C. Light, J. Chem. Phys. **40**, 3221 (1964).
[47] J. C. Light and J. Lin, J. Chem. Phys. **43**, 3209 (1965).
[48] P. Pechukas and J. C. Light, J. Chem. Phys. **42**, 3281 (1965).
[49] T. Su and M. T. Bowers, J. Chem. Phys. **58**, 3027 (1973).
[50] W. J. Chesnavich, T. Su, and M. T. Bowers, J. Chem. Phys. **72**, 2641 (1980).
[51] T. Su and M. T. Bowers, Int. J. Mass. Spectrom. Ion Phys. **12**, 347 (1973).
[52] T. Su, E. C. F. Su, and M. T. Bowers, J. Chem. Phys. **69**, 2243 (1978).
[53] R. N. Dixon, G. Duxbury, J. W. Rabelais, and L. Asbrink, Mol. Phys. **31**, 423 (1976).
[54] J. E. Reutt, L. S. Wang, Y. T. Lee, and D. A. Shirley, J. Chem. Phys. **85**, 6928 (1986).
[55] R. H. Schultz and P. B. Armentrout, J. Chem. Phys. **96**, 1036 (1992).